Crystal structure and electronic properties of bulk and thin film brownmillerite oxides

Joshua Young[1,2,*] and James M. Rondinelli[2,3,†]

[1]*Department of Materials Science and Engineering, Drexel University, Philadelphia, Pennsylvania 19104, USA*

[2]*Department of Materials Science and Engineering, Northwestern University, Evanston, Illinois 60208, USA*

[3]*Materials Science Division, Argonne National Laboratory, Argonne, Illinois 60439, USA*

(Received 7 September 2015; published 17 November 2015)

The equilibrium structure and functional properties exhibited by brownmillerite oxides, a family of perovskite-derived structures with alternating layers of BO_6 octahedra and BO_4 tetrahedra, viz., ordered arrangements of oxygen vacancies, is dependent on a variety of competing crystal-chemistry factors. We use electronic structure calculations to disentangle the complex interactions in two ferrates, $Sr_2Fe_2O_5$ and $Ca_2Fe_2O_5$, relating the stability of the equilibrium (strain-free) and thin film structures to both previously identified and herein newly proposed descriptors. We show that cation size and intralayer separation of the tetrahedral chains provide key contributions to the preferred ground state. We show the bulk ground-state structure is retained in the ferrates over a range of strain values; however, a change in the orientation of the tetrahedral chains, i.e., a perpendicular orientation of the vacancies relative to the substrate, is stabilized in the compressive region. The structure stability under strain is largely governed by maximizing the intraplane separation of the dipoles generated from rotations of the FeO_4 tetrahedra. Lastly, we find that the electronic band gap is strongly influenced by strain, manifesting as an unanticipated asymmetric-vacancy alignment dependent response. This atomistic understanding establishes a practical route for the design of functional electronic materials in thin film geometries.

DOI: 10.1103/PhysRevB.92.174111 PACS number(s): 33.15.Dj, 77.84.Bw, 31.15.A−

I. INTRODUCTION

The family of brownmillerite oxides (general formula $ABO_{2.5}$ or $A_2B_2O_5$) are highly studied for use in ionic conducting and anion insertion applications [1–8]. Their structure type can be thought of as an ABO_3 perovskite with one-sixth of the oxygen atoms removed [Fig. 1(a)], creating parallel rows of ordered anion vacancies along the [110] crystallographic direction; this results in alternating layers of corner-connected BO_4 tetrahedra and BO_6 octahedra [Fig. 1(b)]. Although cooperative distortions and octahedral rotations are well understood in perovskites, the presence of tetrahedral layers in the brownmillerites adds additional structural complexity and possible degrees of freedom for both structure and electronic function design. In addition to rotations of the octahedra, each tetrahedral chain can twist in a left-handed or right-handed sense, resulting in two different types of chains related by a mirror plane perpendicular to the direction of the chain's extension [Fig. 1(c)]. Furthermore, these different chains can be ordered relative to each other within the brownmillerite unit cell, resulting in a variety of structures displaying different space group symmetries.

When the tetrahedra and octahedra are not rotated, the structure displays the *Imma* space group [Fig. 2(a)]; this aristotype may be used as a high symmetry reference phase for which subsequent structural analyses are made. Alternatively, the *Imma* structure can be imagined as having disordered left- and right-handed chains (i.e., the chains display either incommensurate ordering or no long-range order); some structures, such as Sr_2CoFeO_5 and Sr_2MnGeO_5 [9,10], display this phase at ambient conditions, while others become disordered at high temperature (including $Ca_2Al_2O_5$ and $Ca_2Fe_2O_5$) [11,12]. Each of the three low-symmetry bulk hettotypes display two-dimensional sheets of corner-connected octahedra, which rotate out-of-phase along the *ac* direction. This rotation transforms like the irreducible representation (irrep) Γ_1^+ of the *Imma* phase.

Along the *b* axis, however, the allowed displacements of the oxygen atoms are constrained by the handedness and ordering of the tetrahedral chains, which ultimately control the final symmetry of the brownmillerite structure (see the discussion in Sec. III). The tetrahedral chains can cooperatively rotate in a variety of ways, each described by a different irrep of *Imma*. When the tetrahedra rotate into either all left-handed or all right-handed chains the structure displays the polar space group *I*2*bm* owing to the Γ_3^- irrep [Fig. 2(b)]. If there is a racemic mixture of both types of chains, the structure becomes centrosymmetric, with different relative orderings generating different symmetries. Alternating chains of different handedness within each tetrahedral layer is described by the Λ_4 irrep and yields the centrosymmetric *Pbcm* structure [Fig. 2(c)], while alternation between layers (given by X_4^+) gives the centric *Pnma* structure [Fig. 2(d)]. Because the left- and right-handed chains are related by symmetry and differ only by small atomic displacements, the formation energies for the different polymorphs are nearly degenerate and should form with equal probability. However, each of the aforementioned ordering types is seen experimentally in various members of the brownmillerite family, and the driving force behind the preferred type in different chemistries is not completely understood.

Another degree of freedom appears for the brownmillerite structures when the materials are grown as a thin film, e.g., via molecular beam epitaxy or pulsed laser deposition, owing to the constraints imposed by epitaxial strain. In this thin film case, the oxygen-deficient layers can order parallel or perpendicular to the substrate [this is shown in Figs. 3(a) and 3(b), respectively, with the pseudocubic orientation shown

*jy346@drexel.edu

†jrondinelli@northwestern.edu

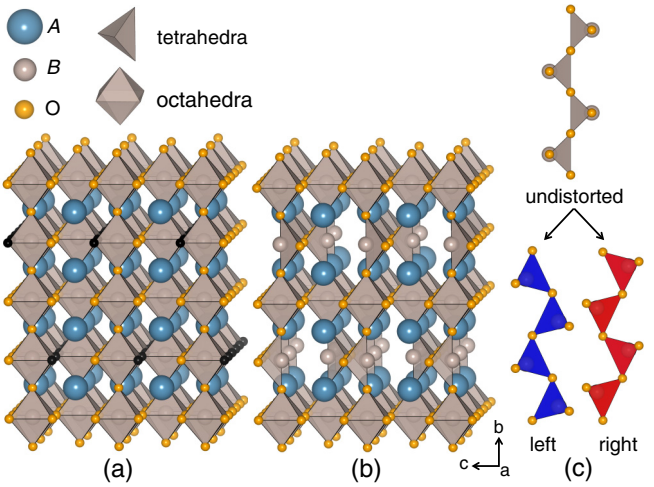

FIG. 1. (Color online) The removal of chains of oxygen atoms (colored in black) from the ABO_3 perovskite structure (a) results in the vacancy ordered $A_2B_2O_5$ brownmillerite structure (b), which consists of alternating layers of BO_4 tetrahedra and BO_6 octahedra along the b direction. The undistorted rows of BO_4 tetrahedra can then twist (c) to create left- or right-handed chains (colored blue and red, respectively).

in Figs. 3(c) and 3(d)]. Although different strain states will stabilize one orientation over the other, it is not always clear which will be preferred and why. In (La,Sr)Co_2O_5,

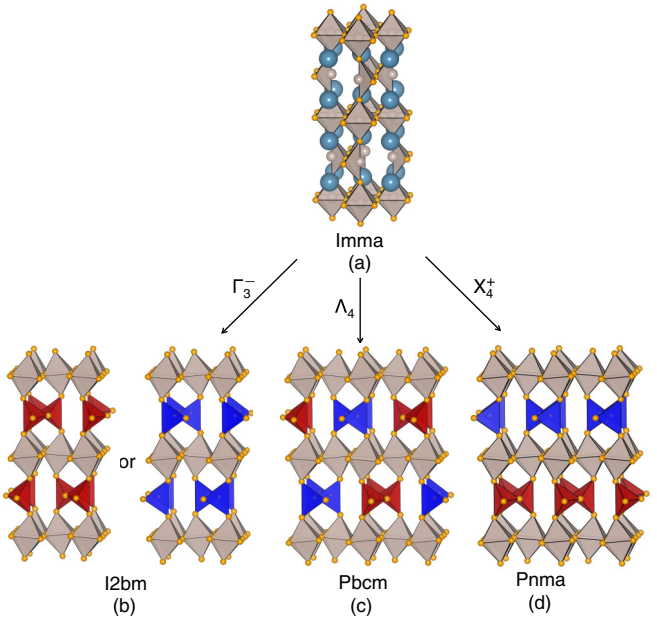

FIG. 2. (Color online) The hypothetical high symmetry brownmillerite structure (a) is defined as having no octahedral or tetrahedral rotations, and has the *Imma* space group. Relative ordering of tetrahedral chains results in three different low-symmetry structures. If all chains are of the same handedness, the structure is polar *I2bm* (b); alternation of left- and right-handed chains within each layer results in centric *Pbcm* (c), while alternation between each layer gives centric *Pnma* (d). The *A*-site cations are omitted from the low-symmetry structures for clarity.

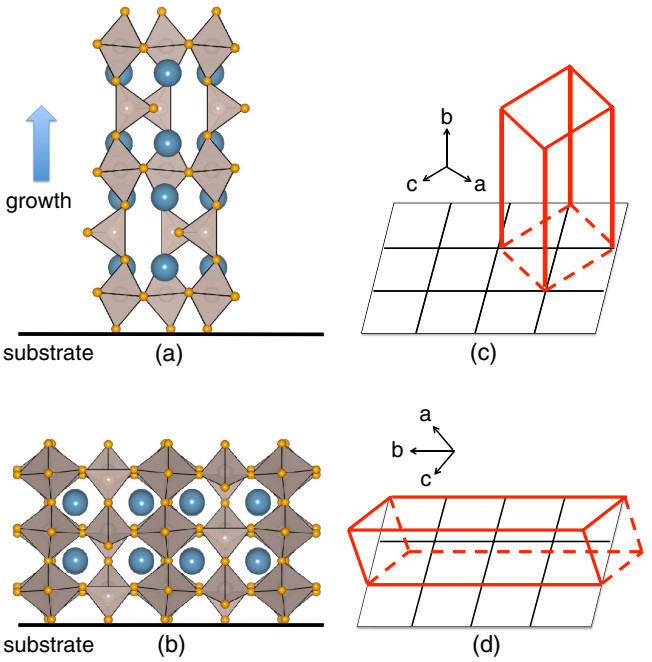

FIG. 3. (Color online) When brownmillerite structures are placed under epitaxial strain, the oxygen-deficient layers can order (a) parallel or (b) perpendicular to the substrate, with the pseudocubic orientations shown in (c) and (d), respectively.

for example, tensile strain stabilizes perpendicular ordering while compressive strain stabilizes parallel ordering [13,14]; however, the opposite effect is observed in strained $Ca_2Fe_2O_5$ [15].

In this work, we seek to disentangle the structural and energetic effects operative in brownmillerite oxides through an investigation of bulk and epitaxially strained $Sr_2Fe_2O_5$ and $Ca_2Fe_2O_5$ using first-principles density-functional theory calculations. The $Sr_2Fe_2O_5$ and $Ca_2Fe_2O_5$ members are experimentally known to be stable in the ordered brownmillerite phase up to high temperatures (approximately 1200 K for $Sr_2Fe_2O_5$ and 920 K for $Ca_2Fe_2O_5$) [16,17]; at ambient conditions, $Sr_2Fe_2O_5$ displays the *Pbcm* ordering [18,19], while $Ca_2Fe_2O_5$ exhibits the *Pnma* structure [17]. Additionally, they both contain only Fe^{3+} cations and display *G*-type antiferromagnetic ordering with high Néel temperatures (700 and 720 K, respectively) [16,20,21]. The indirect band gap of both compounds is approximately 2.0 eV, owing to a Γ- to *X*-point transition [22].

We find that, in agreement with experimental results of the bulk phases, the *Pbcm* and *Pnma* phase are the lowest energy (and thus equilibrium) structures for $Sr_2Fe_2O_5$ and $Ca_2Fe_2O_5$, respectively. Furthermore, we find that the parallel (or perpendicular) ordering is preferred under tensile (or compressive) strain; additionally, this structural stability switch occurs due to which ordering maximizes the intralayer tetrahedral chain distance under a specific strain state, analogously to the bulk phases. Finally, we report that the band gap of these materials is also influenced by epitaxial strain owing to strain-induced changes to the intralayer bond angles. Although strain is well known to influence the band gap via control of the octahedral rotations in ABO_3 perovskites, the alternating

octahedra-tetrahedra layers in the brownmillerites allow for a more complex coupling between the two. We show that, similar to the ABO_3 perovskites, an alteration of the B-O-B bond angles causes this response; unlike perovskites, however, it is the angle between the tetrahedrally and octahedrally coordinated B cations that controls the band gap. The band gap of the compounds in the parallel orientation increases under increasing tensile strain, but decreases in the perpendicular orientation, a discrepancy that arises from how the response of the out-of-plane lattice parameter to strain affects this bond angle differently in the two orientations.

II. COMPUTATIONAL METHODS

All investigations were performed using density-functional theory as implemented in the Vienna *ab initio* simulation package (VASP) [23–25]. We used projector augmented-wave (PAW) potentials with the PBEsol functional [26,27], chosen because it is a type of GGA functional adjusted to give better agreement with lattice parameters and bond angles specifically in solids, with valence electron configurations of $3s^2 3p^6 4s^2$ for Ca, $4s^2 4p^6 5s^2$ for Sr, $3d^7 4s^1$ for Fe, and $2s^2 2p^4$ for O. A plane-wave cutoff of 500 eV and a $7 \times 5 \times 7$ Monkhorst-Pack mesh was used during the structural relaxations [28]. We applied a Hubbard-U correction of 5 eV using the Dudarev formalism to treat the correlated Fe $3d$ states; this value gives good agreement between the computed and experimental band gap of these ferrates. Note that the structural parameters were found to be less sensitive to the choice of U; for example, the b lattice parameter of relaxed $Sr_2Fe_2O_5$ ($Pbcm$ symmetry) obtained with $U = 3$ eV and $U = 5$ eV differed by less than 0.02% and the Fe-O-Fe tetrahedral bond angles differed by 0.6°. In all calculations, we also enforced a G-type antiferromagnetic collinear spin ordering on the Fe atoms [29]. Symmetry-adapted mode decompositions were performed using the ISODISTORT tool, part of the ISOTROPY software suite [30]. Atomic structures were visualized using VESTA [31].

To simulate the application of epitaxial strain by growth on a cubic [001] terminated perovskite substrate with a square surface net, we fix the in-plane a and c lattice parameters to be equal and allow the out-of-plane b axis and ions to fully relax (adopted from the approach of Ref. [32]). The $I2bm$, $Pbcm$, and $Pnma$ phases of $Ca_2Fe_2O_5$ and the $I2bm$ and $Pbcm$ phases of $Sr_2Fe_2O_5$, in both the parallel and perpendicular orientation were strained from −3 to 3% in increments of 1%. Because of the difference in size and equilibrium volume of the $Ca_2Fe_2O_5$ and $Sr_2Fe_2O_5$ unit cells, application of the same percent strain results in different pseudocubic lattice parameters (a_{pc}) for the two structures; for this reason, we report the strain in terms of a_{pc} rather than in terms of percentage.

III. RESULTS AND DISCUSSION

A. Polyhedral rotation definitions

To characterize the brownmillerite structures, we consider three types of rotation angles: the angle between (i) the FeO_4 tetrahedra (Θ_T), (ii) the FeO_6 octahedra (Θ_O), and (iii) the tetrahedra and octahedra (Θ_{OT}). We report these angles as

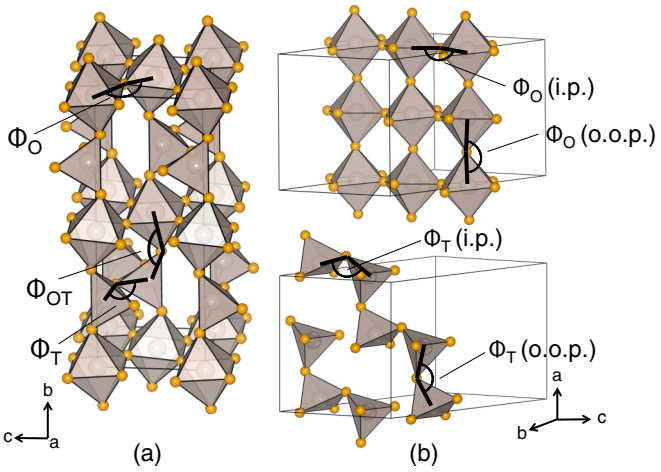

FIG. 4. (Color online) (a) The three characteristic angles of the $A_2B_2O_5$ brownmillerite structure. Rotations of the tetrahedral chains, of the octahedral network, and between the tetrahedral and octahedral layers are given by Φ_T, Φ_O, and Φ_{OT}, respectively. These three angles are sufficient to describe the case when the tetrahedral chains order parallel to the substrate under biaxial strain. In (b) the perpendicular orientation, however, the changes in the out-of-plane lattice parameter owing to the strain state split the octahedral and tetrahedral rotation angles.

$\Theta_X = (180 - \Phi_X)/2$, where the definition of Φ_X ($X = T$, O, or OT) is shown in Fig. 4; in this case, a larger angle indicates a larger distortion of the relative bonds away from 180°. In the bulk case, and the case of parallel orientation of vacancies under strain, these three angles are sufficient to describe the structure [Fig. 4(a)]. In the perpendicular orientation, however, the applied strain and response of the out-of-plane lattice parameter now affect the tetrahedra and octahedra in different ways. To capture this, we divide Φ_O and Φ_T into two unique angles defined by in-plane (i.p.) and out-of-plane (o.o.p.) components [Fig. 4(b)].

B. Bulk phases

We first investigated the bulk phases of $Sr_2Fe_2O_5$ and $Ca_2Fe_2O_5$ with the three tetrahedral chain orderings shown in Fig. 2. The main results are summarized in Table I. In the case of $Sr_2Fe_2O_5$, we found that centrosymmetric $Pbcm$ is the lowest-energy structure, followed by $I2bm$, with $Pnma$ being the highest. In $Ca_2Fe_2O_5$, we found the $Pnma$ structure to be lowest in energy, followed by $I2bm$ and $Pbcm$. Each polymorph is separated from the other two by a small amount of energy (ΔE, Table I), indicating that the formation of a right- or left-handed tetrahedral chain may be equally probable. Furthermore, the lattice parameters, rotation angles, and band gaps vary only slightly between orderings. Between the two chemistries, $Ca_2Fe_2O_5$ has a smaller unit cell and larger rotation angles than $Sr_2Fe_2O_5$, which is due to the smaller size of the Ca^{2+} cation.

Experimentally, the structure of $Sr_2Fe_2O_5$ has been highly contested. Initial structure refinements on powder samples ambiguously supported assignment of both completely disordered tetrahedral chains (space group $Imma$) or pure left- or

TABLE I. The energetics and structure of bulk $Sr_2Fe_2O_5$ and $Ca_2Fe_2O_5$. The tolerance factor (τ) is defined by Eq. (2) in the text. The energy difference between the different tetrahedral chain-ordering structures is given as ΔE; each energy is given as the difference in meV between that phase and the lowest energy phase for each compound normalized to the number of formula units. The a, b, and c lattice parameters are given in Å. The rotations of the tetrahedra, octahedra, and between the octahedra and tetrahedra are given in degrees as Θ_T, Θ_O, and Θ_{OT}, respectively; each is defined in Fig. 4. The average intralayer separation of tetrahedral chains is R (defined in Fig. 5), and the deviation in the bond lengths of an octahedra is given by Δ. The band gap (E_g) of each structure is given in eV.

$Sr_2Fe_2O_5$ ($P_T = 3.8$ D, $\tau = 0.976$)										
Symmetry	ΔE (meV/f.u.)	a (Å)	b (Å)	c (Å)	Θ_T (°)	Θ_O (°)	Θ_{OT} (°)	R (Å)	Δ ($\times 10^{-4}$)	E_g (eV)
I2bm	12.6	5.501	15.402	5.659	24.48	3.70	15.41	5.0977	18.79	2.19
Pbcm	0	5.503	15.407	11.311	24.54	4.43	15.39	5.0988	19.07	2.15
Pnma	22.7	5.499	15.413	5.659	24.49	3.64	15.31	5.0971	19.03	2.09
$Ca_2Fe_2O_5$ ($P_T = 1.7$ D, $\tau = 0.923$)										
Symmetry	ΔE (meV/f.u.)	a (Å)	b (Å)	c (Å)	Θ_T (°)	Θ_O (°)	Θ_{OT} (°)	R (Å)	Δ ($\times 10^{-4}$)	E_g (eV)
I2bm	16.7	5.381	14.617	5.579	27.92	6.538	20.34	5.0173	11.16	2.16
Pbcm	23.3	5.386	14.627	11.155	28.16	4.909	19.90	5.0476	10.85	2.13
Pnma	0	5.397	14.632	5.561	27.23	8.032	20.45	4.9941	10.73	2.07

right-handed ordering (space group *I2bm*); this material was thus theorized to display *I2bm* symmetry locally, but with random ordering taking place over longer length scales. This was challenged, however, by transmission electron microscopy results showing clear intralayer alternation of tetrahedral chains [33]. Additionally, more recent neutron diffraction experiments on single crystals grown by the floating zone method have indicated that *Pbcm* is indeed the preferred structure type for $Sr_2Fe_2O_5$ [18,19]. Furthermore, all of these recent experiments are supported by the aforementioned results of our *ab initio* calculations; the small energy difference between the *Pbcm* and *I2bm* structures, however, indicate that intergrowths of the phases is not out of the question. In contrast to the ambiguity of $Sr_2Fe_2O_5$, the structure of $Ca_2Fe_2O_5$ is well known to form in the *Pnma* phase [17], again in agreement with our theoretical results.

What factors lead to and stabilize the preferred ground state in different brownmillerite compounds? In 2005, Abakumov *et al.* put forth the idea that the twisting of tetrahedral chains away from the undistorted 180° orientation creates local dipole moments, with larger rotations producing larger dipoles [34]. Hadermann and Abakumov *et al.* further suggested that the distance between the tetrahedral layers (i.e., the length of the *b* axis) is also an important factor to consider [35]. Parsons *et al.* then recognized that each tetrahedral ordering scheme distorts the octahedra in different ways; the fact that the octahedra are not connected out-of-plane (along *b*) causes the apical oxygen atoms to displace more than the equatorial ones, which creates a shearing effect from this nonrigid rotation. Generally, the *I2bm* phase causes the least octahedral (elastic) distortion, followed by *Pnma*, with *Pbcm* causing the most distortion. These arguments were then used to construct a structure map relating the observed phase of different brownmillerites to these factors, followed by a classification of several known compounds into this scheme [36]. Although these observations have been key in building an understanding of structural trends in brownmillerite oxides, and are corroborated by some recently synthesized brownmillerite phases (such as $Ca_2Cr_2O_5$) [37], discrepancies in this structure map show there are additional effects, which should be considered. Ca_2FeCoO_5 and $Ca_2Co_2O_5$, for example, both display the *Pbcm* rather than the structure map predicted *Pnma* geometry [38,39].

We now seek to explain the stability of these materials' preferred ground-state phase in terms of local structure. The tetrahedral chain ordering configuration preferred by the ground state can be summarized as a complex competition between two primary energetic factors: (i) separation of the tetrahedral chains (i.e., minimization of electrostatic repulsion) and (ii) distortion of the nominally regular BO_6 octahedra (minimization of elastic strain energy). The three different ordering schemes shown in Fig. 2 better maximize either factor (i) or (ii), at the expense of the other.

Following the approach of Zhang *et al.* [39], we can assign a magnitude to the local dipole generated by the tetrahedral rotations (P_T, Table I, given in units of Debye). P_T is calculated based on the Debye equation, $\mu = neR$, where μ is the net dipole moment, n is the number of electrons, e is the elementary charge, and R is the distance between centers of charge; following the approach of Poeppelmeier *et al.*, we estimated the distribution of electrons using bond valence sums [40]. In compounds with large P_T, factor (i) becomes the quantity of interest to maximize; rather than considering the separation along *b*, however, we quantify this by defining the average intralayer separation of the tetrahedral chains as R (shown in Fig. 5). Competing with this is factor (ii), i.e., the regularity in the octahedra. We use the averaged sum-of-squares difference between the measured bond lengths (d_n) and the average bond length (d_{avg}) in the octahedra to quantify this:

$$\Delta = \frac{1}{N}\sum_{i=1}^{n}\left(\frac{d_n - d_{\text{avg}}}{d_{\text{avg}}}\right)^2. \quad (1)$$

For small values of P_T, factor (ii) becomes the critical quantity to optimize, and minimizing Δ becomes more important than maximizing R.

Interestingly, we found that although $Sr_2Fe_2O_5$ has smaller rotations, it has a larger chain dipole ($P_T = 3.8$D) than $Ca_2Fe_2O_5$ ($P_T = 1.7$D); generally, one would expect smaller rotations to generate a smaller dipole. This is due to the fact

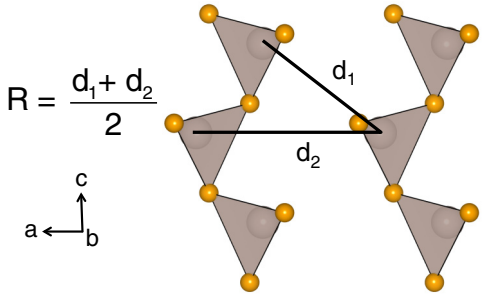

FIG. 5. (Color online) The intralayer chain separation in the brownmillerite structure. The average separation distance is given by R, which is defined as the average of the two distances between Fe atoms of different chains (d_1 and d_2).

that the electric polarization generated by the apical oxygen atoms tends to cancel that from the equatorial oxygen atoms in the tetrahedra; however, the smaller rotations of the octahedra in $Sr_2Fe_2O_5$ means this cancellation happens to a lesser degree, increasing P_T. Again, at large values of P_T, the need to separate the dipoles, factor (i), overcomes the need to have regular octahedra, factor (ii). $Sr_2Fe_2O_5$ therefore exhibits the $Pbcm$ structure, which allows for the best average in-plane separation (R, Table I) of the large dipoles. In $Ca_2Fe_2O_5$, the larger octahedral rotations distort the octahedra more in the presence of tetrahedral chains; this, in combination with the small chain dipole, therefore gives more importance to the phase that keeps the octahedra most regular (Δ, Table I). In this case, that is the $Pnma$ structure.

Another approach to understanding these energetic competitions is to consider the the Goldschmidt tolerance factor [41]. This quantity is given by:

$$\tau = \frac{r_A + r_O}{\sqrt{2}(r_B + r_O)}, \quad (2)$$

where r_A, r_B, and r_O is the radius of the A-site atom, B-site atom, and oxide anion, respectively [42]. An ideal undistorted (cubic or tetragonal) structure will have $\tau = 1$; the further the tolerance factor deviates from 1, the more the structure is likely to distort, and the larger the octahedral rotations will be. In $Ca_2Fe_2O_5$ ($\tau = 0.923$), the $Pnma$ phase least distorts the octahedra (as reflected in Δ in Table I), and is therefore the most stable. As τ increases, the need to maximize the separation between dipoles overcomes the steric packing driving force for octahedral rotations and hence they decrease; because $Pbcm$ best maximizes this distance (R in Table I), it is the preferred phase for the larger $Sr_2Fe_2O_5$ ($\tau = 0.976$).

Finally, despite the structural differences between the bulk $Sr_2Fe_2O_5$ and $Ca_2Fe_2O_5$ phases, the DFT-PBEsol (indirect $\Gamma - X$) band gap remains nominally the same (~2.10 eV) across changes in chemistry and tetrahedral ordering. This is due to the fact that O $2p$ states make up the top of the valence band, while the bottom of the conduction band is made up of Fe $3d$ states, making the band gap largely independent of A-site chemistry. A more detailed analysis of the changes in the electronic gap is given for the thin film cases below.

C. Strained phases

We next investigated the crystal and electronic structure of $Sr_2Fe_2O_5$ and $Ca_2Fe_2O_5$ under epitaxial strain. As mentioned previously, we must now consider the orientation of the vacancies as another degree of freedom (i.e., whether the vacancy layers are parallel or perpendicular to the substrate, Fig. 3), in addition to tetrahedral chain rotation and ordering. First, we find that when $Sr_2Fe_2O_5$ is constrained to a substrate, it retains the $Pbcm$ ground state in both parallel (filled symbols) and perpendicular (empty symbols) substrate-vacancy orientations [Fig. 6(a), top], a fact that can be explained using the same arguments presented for the bulk phase. However, we also find that the perpendicular configuration of oxygen-deficient layers is stabilized over the parallel arrangement under small amounts of compressive strain. This is due to the fact that increasing compressive strain decreases the intralayer separation between tetrahedral chains if the vacancies are ordered parallel to the substrate (i.e., becomes more energetically unfavorable), but increases R if the vacancies are perpendicular. The strain value at which the perpendicular ordering becomes more stable exactly coincides with the values at which the intralayer separation becomes greater [Fig. 6(a), middle] and the octahedral distortions become smaller [Fig. 6(a), bottom] than that of the parallel ordering.

One important detail to note is that $Sr_2Fe_2O_5$ has a relatively large pseudocubic lattice parameter (a_{pc}); only with some of the largest commercially available substrates can it be placed under tensile strain and have the parallel orientation be stabilized. Many experimental observations agree with our prediction of the energetic stability of vacancy orientation. Growth of $Sr_2Fe_2O_5$ near the transition point, such as on $SrTiO_3$ ($a_{pc} = 3.91$ Å) shows a competition between the two orientations [43], whereas growth on larger substrates stabilizes the parallel orientation, such as on $KTaO_3$ ($a_{pc} = 3.99$ Å) [44].

When $Ca_2Fe_2O_5$ is placed under epitaxial strain, the $Pnma$ phase remains lowest in energy, while the $I2bm$ and $Pbcm$ structures become much closer in energy and strongly compete. As with $Sr_2Fe_2O_5$, the tetrahedral layers in $Ca_2Fe_2O_5$ switch to a perpendicular orientation under compressive strain, and parallel under tensile [Fig. 6(b), top]. Once again, this occurs due to the perpendicular orientation maximizing the distance R between intralayer tetrahedral chains and minimizing octahedral distortions, Δ, under compression [Fig. 6(b), middle and bottom]. Although the $Pnma$ phase minimizes octahedral shearing as in the bulk phase, the very small differences in Δ between the strained phases means that it cannot be the only controlling feature; instead there is a complex interplay between the various structural descriptors that produces the observed ground state. The fact that $Ca_2Fe_2O_5$ has a smaller pseudocubic lattice parameter than $Sr_2Fe_2O_5$ means that the parallel phase is experimentally accessible with much more modest strain. Experimental results on thin films of $Ca_2Fe_2O_5$ show that the vacancies order perpendicularly when grown on $LaSrAlO_4$ (LSAO, $a_{pc} = 3.75$ Å) and $LaAlO_3$ ($a_{pc} = 3.79$ Å), but order parallel on LSAT ($a_{pc} = 3.87$ Å) and $SrTiO_3$ ($a_{pc} = 3.91$ Å), again in agreement with these theoretical results [15,45]. Interestingly, the stabilization of the perpendicular phase under compressive

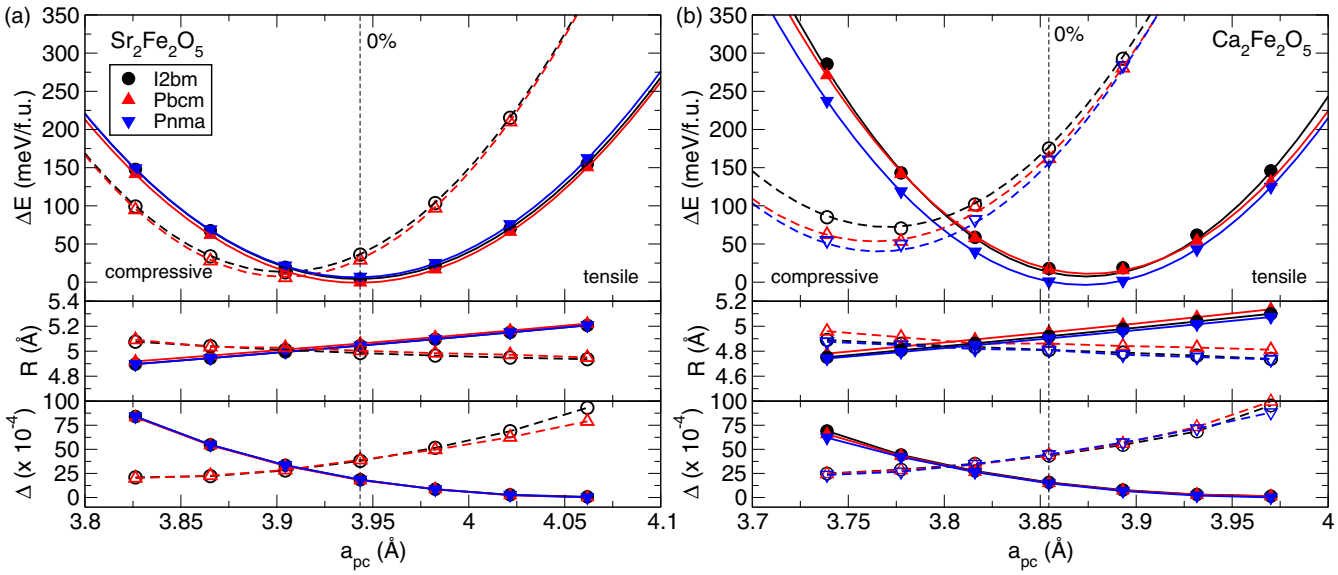

FIG. 6. (Color online) Energy of the different tetrahedral chain ordered $Sr_2Fe_2O_5$ (a) and $Ca_2Fe_2O_5$ (b) structures as a function of epitaxial strain (top panels). In both cases, the parallel vacancy ordering (filled symbols) is stabilized under tensile strain, while perpendicular (empty symbols) is stabilized under compressive. This change in stabilization occurs at the point where either the parallel or perpendicular phase maximizes the average intralayer tetrahedral chain separation (R, middle panels) and minimizes the octahedral distortion effect (Δ, bottom panels).

strain and parallel phase under tensile strain does not hold across all brownmillerite oxide chemistries; in the cobaltates, for example, the trend is reversed.

We next examined the structural evolution of these compounds under strain. For the structures with the parallel orientation, there are only the three bond angles defined previously to consider (Fig. 4). Under increasing tensile strain, the FeO_4 tetrahedral chains become less distorted (decreasing Fe-O-Fe bond angle), while the octahedral network and connections between the tetrahedral and octahedral layers, become more distorted (increasing Fe-O-Fe bond angle). It should come as no surprise that this trend holds across all three types of ordered phases, as they are all structurally very similar with the exception of the relative orientation of tetrahedral chains (Fig. 7). Additionally, the chemistry of the A site, although influencing the magnitude of the tilts, does not affect this trend.

When the oxygen-deficient layers reorient to become perpendicular to the substrate, there are now two more angles to consider. In the previous geometries, only one angle of the tetrahedra and octahedra had to be considered owing to the fact that the equatorial oxygen atoms of each were in the plane of epitaxial strain. Now these same atoms are oriented such that they are affected by both the plane of epitaxial strain and the strain-induced changes to the out-of-plane lattice parameter. In order to get a full understanding of the structural distortions in this case, we separate the tetrahedral and octahedral angles into in-plane and out-of-plane components. In this perpendicular orientation, increasing tensile strain increases the out-of-plane component of the octahedral and tetrahedral angles, while decreasing the in-plane component, as well as the angle between the layers.

Finally, the band gap of both materials is strongly influenced by strain, ranging from 1.8–2.6 eV for $Sr_2Fe_2O_5$ [Fig. 8(a)] and 1.6 –2.5 eV for $Ca_2Fe_2O_5$ [Fig. 8(b)]. In both compounds, increasing tensile strain results in an increase of the band gap for the parallel orientation of vacancies, but interestingly, a decrease in the perpendicular orientation. This is due to how an increase in the lattice parameters influences the connectivity of the tetrahedrally and octahedrally coordinated iron atoms (i.e., Θ_{OT}). For the films with the parallel vacancy orientation, Θ_{OT} deviates further away from 180° as tensile strain increases; this results in decreased overlap of the Fe d orbitals and O p orbitals, giving a higher band gap. Figures 8(c) and 8(d) show, as an example, the difference in the band gap of parallel-oriented $Sr_2Fe_2O_5$ at 2% (2.43 eV) and −2% (2.00 eV) strain. The opposite effect occurs in the perpendicular case, where a decrease in Θ_{OT} provides better overlap and thus a smaller band gap through increased bandwidth.

D. Comparison to perovskite oxides

The fact that BO_6 octahedra in perovskite oxides form a flexible corner-connected network [Fig. 1(a)] allows them to easily rotate in space about the different crystallographic axes. The size of these rotations directly affect the magnitude of the B-O-B bond angles, which in turn impacts many electronic and magnetic properties. Although there are 15 distinct ways in which the octahedra can cooperatively rotate while retaining connectivity (as identified by Glazer) [46], the vast majority exhibit either an orthorhombic or rhombohedral tilt pattern (given by $a^-a^-c^+$ or $a^-a^-a^-$ in Glazer notation, respectively). A high degree of control over the electronic structure can be achieved by using epitaxial strain (or chemical substitution, as captured by τ) to control these rotations, owing primarily to the strong coupling between the lattice and electronic degrees of freedom in perovskites [Fig. 9(a)] [47–50]; as mentioned previously, buckling of

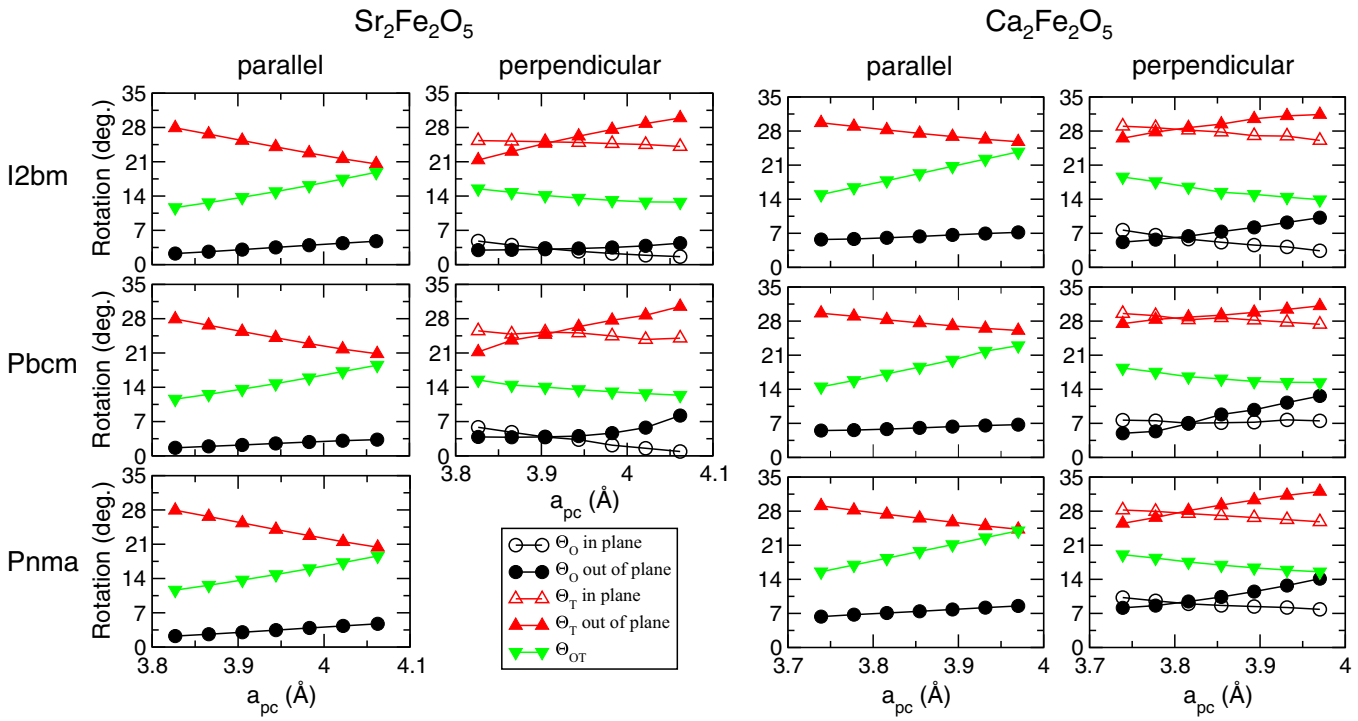

FIG. 7. (Color online) The effect of strain on the tilt angles (as defined in Fig. 4) of the different $Sr_2Fe_2O_5$ (left) and $Ca_2Fe_2O_5$ (right) structures with both parallel and perpendicular vacancy orientation.

the B-O-B bond away from a linear 180° configuration (i.e., increasing the magnitude of the octahedral rotations) decreases the overlap between the O p and metal B d orbitals, thereby increasing the band gap in insulating compounds or inducing bandwidth-driven metal-insulator transitions [51–56].

As we have shown, the distinct alternating tetrahedral and octahedral layers in brownmillerites allow for many more structural degrees of freedom than perovskites. Application of the same forces (chemical pressure and epitaxial strain) now affects the interlayer separation of tetrahedra (i.e., b lattice parameter), as well as the rotations (connectivity) of the different polyhedra (given by Θ_O, Θ_T, and Θ_{OT}); each of these in turn influences the octahedral distortions (Δ), the intralayer dipole separation (R), and the magnitude of the local tetrahedral dipoles (P_T). The balance of these different factors, which is shown schematically in Fig. 9(b), is then what governs the equilibrium structure—the tetrahedral chain

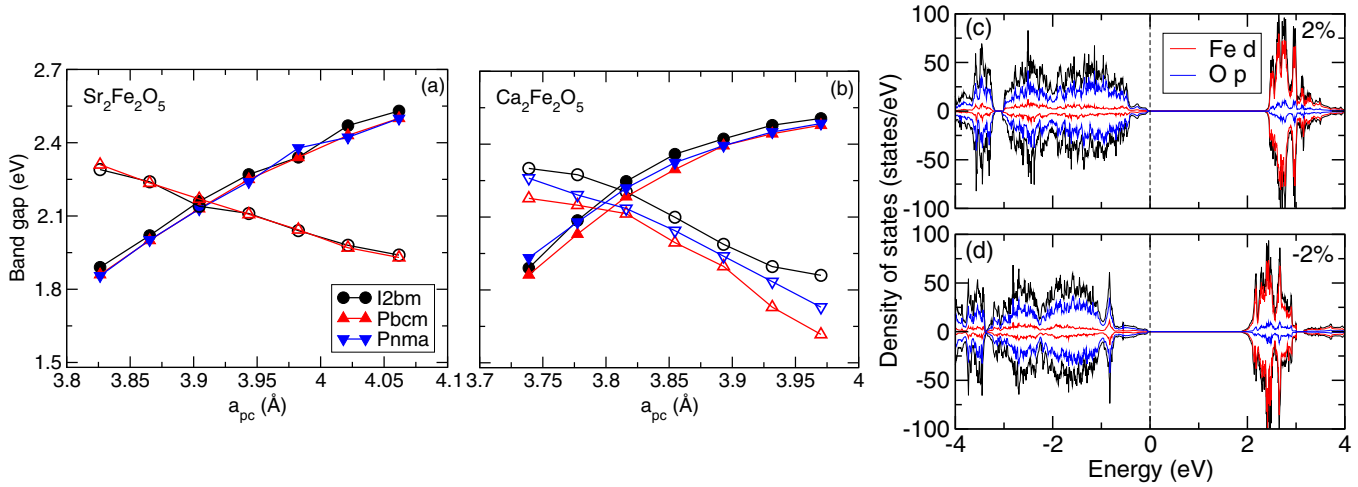

FIG. 8. (Color online) The band gap of (a) $Sr_2Fe_2O_5$ and (b) $Ca_2Fe_2O_5$ are strongly influenced by epitaxial strain; the electronic gap for thin film structures with vacancies ordered parallel to the substrate (filled symbols) increases as tensile strain increases, but decreases in the perpendicular orientation (empty symbols). This electronic structure response occurs owing to the manner in which strain affects the angle between the tetrahedral and octahedral layers. The *Pbcm* structure of $Sr_2Fe_2O_5$ with vacancies parallel to the substrate, for example, has a ~0.3 eV larger band gap under (c) 2% tensile strain when compared to (d) 2% compressive strain as seen by the change in the atom-resolved densities of states.

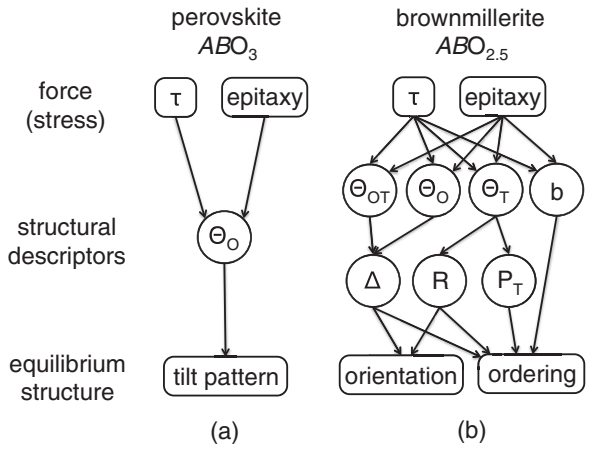

FIG. 9. The effect of different stress stimuli [ionic size or chemical pressure (captured by τ) and epitaxy] on various structural descriptors, which combine to produce the equilibrium crystal structure in (a) perovskite and (b) brownmillerite oxides.

ordering and, for the case of thin films, the orientation of the vacancies relative to the substrate.

A feature implicitly indicated in Fig. 9 is that the electronic properties of these oxides are also a structural consequence; hence, control over the structural descriptors makes it possible to control the electronic response. Indeed, the band gaps of the brownmillerites are highly sensitive to rotations of the polyhedra; like the perovskites, the gap opens as the rotations increase owing to a change in orbital overlap. Unlike perovskites, however, it is not solely a single B-O-B bond angle controlling the electronic structure, which is due to the breaking of the structural topology by the oxygen-vacant (tetrahedral) layers. For the brownmillerite oxides, it is the out-of-plane angle between the BO_4 tetrahedra and BO_6 octahedra, given by Θ_{OT} (or, alternatively, B_{tet}-O-B_{oct}), that controls the gap and band-edge character. Furthermore, strain affects the band gap of parallel or perpendicularly oriented brownmillerites in opposite (asymmetric) ways owing to the response of Θ_{OT} to the biaxial strain state. Although strain has been used to control functional properties in perovskites, it appears it could induce even more interesting responses in brownmillerites owing to the additional structural degrees of freedom present.

IV. CONCLUSION

Using first-principles density-functional theory calculations, we investigated the brownmillerite compounds $Sr_2Fe_2O_5$ and $Ca_2Fe_2O_5$. These anion-deficient materials offer many more degrees of freedom than the related perovskite structures, increasing the structural complexity greatly. The symmetry of these structures is determined by the relative ordering of left- and right-handed tetrahedral chains; which ordering scheme is preferred, however, is determined by the interplay of several structural factors. Although previous studies have attempted to characterize the various members of this family, here we clearly demonstrate how the tolerance factors, dipoles generated by rotations of FeO_4 tetrahedra, distortions of FeO_6 octahedra, and intralayer chain separation interact to produce the observed equilibrium phases.

Furthermore, we show the crystal and electronic structure of these phases are highly tunable using epitaxial strain. We find that under compressive strain, the preferred ordering of vacancies (tetrahedral FeO_4 chains) changes from parallel to perpendicular when the separation between the change becomes better maximized. The rotation angles are also strongly altered, resulting in an increase (or decrease) in the band gap for the parallel (or perpendicular) orientation. Although this study is by no means comprehensive in scope, we hope that the framework presented here encourages the consideration of additional structural features (especially intralayer separation) in future investigations and helps provide greater insight into this and other layered oxide families. We can now harness this knowledge and understanding of the atomistic mechanisms behind the coupling of the crystal and electronic structure in brownmillerites to design electronic function and realize new materials platforms for thin film devices.

ACKNOWLEDGMENTS

We wish to thank members of the Materials Theory and Design Group, as well as D. Fong and J. Zhang, for useful discussions. J.Y. and J.M.R. were supported by the U.S. DOE, Office of Basic Energy Sciences (BES), DE-AC02-06CH11357. DFT calculations were performed on hardware supported by Drexel's University Research Computing Facility, and the CARBON cluster at the Center for Nanoscale Materials (Argonne National Laboratory, also supported by DOE-BES DE-AC02-06CH11357) under allocation CNM39812.

[1] K. R. Kendall, C. Navas, J. K. Thomas, and H.-C. zur Loye, Recent developments in perovskite-based oxide ion conductors, Solid State Ionics **82**, 215 (1995).

[2] J. C. Boivin and G. Mairesse, Recent material developments in fast oxide ion conductors, Chem. Mater. **10**, 2870 (1998).

[3] A. Rolle, R. N. Vannier, N. V. Giridharan, and F. Abraham, Structural and electrochemical characterisation of new oxide ion conductors for oxygen generating systems and fuel cells, Solid State Ionics **176**, 2095 (2005).

[4] A. L. Shaula, Y. V. Pivak, J. C. Waerenborgh, P. Gaczyñski, A. A. Yaremchenko, and V. V. Karton, Ionic conductivity of brownmillerite-type calcium ferrite under oxidizing conditions, Solid State Ionics **177**, 2923 (2006).

[5] A. Orera and P. R. Slater, New chemical systems for solid oxide fuel cells, Chem. Mater. **22**, 675 (2010).

[6] E. V. Antipov, A. M. Abakumov, A. M. Alekseeva, M. G. Rozova, J. Hadermann, O. I. Lebedev, and G. Van Tendeloo, Oxygen and fluorine doping in Sr_2MnGaO_5 brownmillerite, Phys. Status Solidi A **201**, 1403 (2004).

[7] E. Sullivan and C. Greaves, Fluorine insertion reactions of the brownmillerite materials $Sr_2Fe_2O_5$, Sr_2CoFeO_5, and $Sr_2Co_2O_5$, Mater. Res. Bull. **47**, 2541 (2012).

[8] N. A. Tarasova, Y. V. Filinkova, and I. E. Animitsa, Electric properties of oxyfluorides $Ba_2In_2O_{5-0.5x}F_x$, Russ. J. Electrochem. **49**, 45 (2013).

[9] P. D. Battle, T. C. Gibb, and P. Lightfoot, The crystal and magnetic structures of Sr_2CoFeO_5, J. Solid State Chem. **76**, 334 (1988).

[10] A. M. Abakumov, A. M. Alekseeva, M. G. Rozova, E. V. Antipov, O. I. Lebedev, and G. V. Van Tendeloo, Ordering of the tetrahedral chains in the Sr_2MnGaO_5 brownmillerite, J. Solid State Chem. **174**, 319 (2003).

[11] B. Lazic, H. Krüher, V. Kahlenberg, J. Konzett, and R. Kaindl, Incommensurate structure of $Ca_2Al_2O_5$ at high temperatures–structure investigation and raman spectroscopy, Acta Cryst. **B64**, 417 (2008).

[12] H. Krüger and V. Kahlenberg, Incommensurately modulated ordering of tetrahedral chains in $Ca_2Fe_2O_5$ at elevated temperatures, Acta Cryst. **B61**, 656 (2005).

[13] D. O. Klenov, W. Donner, B. Foran, and S. Stemmer, Impact of stress on oxygen vacancy ordering in epitaxial $La_{0.5}Sr_{0.5}CrO_{3-\delta}$ thin films, Appl. Phys. Lett. **82**, 3427 (2003).

[14] J. Gazquez, S. Bose, M. Sharma, M. A. Torija, S. J. Pennycook, C. Leighton, and M. Varela, Lattice mismatch accommodation via oxygen vacancy ordering in epitaxial $La_{0.5}Sr_{0.5}CrO_{3-\delta}$ thin films, APL Mater. **1**, 012105 (2013).

[15] S. Inoue, M. Kawai, N. Ichikawa, H. Kageyama, W. Paulus, and Y. Shimakawa, Anisotropic oxygen diffusion at low temperature in perovskite-structure iron oxides, Nature Chem. **2**, 213 (2010).

[16] M. Schmidt and S. J. Campbell, Crystal and magnetic structures of $Sr_2Fe_2O_5$ at elevated temperatures, J. Solid State Chem. **156**, 292 (2001).

[17] H. Krüger, V. Kahlenberg, V. Petříček, F. Phillipp, and W. Wertl, High-temperature structural phase transition in $Ca_2Fe_2O_5$ studied by in-situ x-ray diffraction and transmission electron microscopy, J. Solid State Chem. **182**, 1515 (2009).

[18] J. E. Auckett, A. J. Studer, N. Sharma, and C. D. Ling, Floating-zone growth of brownmillerite $Sr_2Fe_2O_5$ and the observation of a chain-ordered superstructure by single-crystal neutron diffraction, Solid State Ionics **225**, 432 (2012).

[19] J. E. Auckett, A. J. Studer, E. Pellegrini, J. Ollivier, M. R. Johnson, H. Schober, W. Miiller, and C. D. Ling, Combined experimental and computational study of oxide conduction dynamics in $Sr_2Fe_2O_5$ brownmillerite, Chem. Mater. **25**, 3080 (2013).

[20] T. Takeda, Y. Yamaguchi, S. Tomiyoshi, M. Fukase, M. Sugimoto, and H. Yamamoto, Magnetic structure of $Ca_2Fe_2O_5$, J. Phys. Soc. Jpn. **24**, 446 (1968).

[21] T. Takeda, Y. Yamaguchi, J. Watanabe, S. Tomiyoshi, and H. Yamamoto, Crystal and magnetic structures of $Sr_2Fe_2O_5$, J. Phys. Soc. Jpn. **26**, 1320 (1969).

[22] V. R. Galakhov, E. Z. Kurmaev, K. Kuepper, M. Neumann, J. A. McLeod, A. Moewes, I. A. Leonidov, and V. L. Kozhevnikov, Valence band structure and x-ray spectra of oxygen-deficient ferrites $SrFeO_x$, J. Phys. Chem. C **114**, 5154 (2010).

[23] P. Hohenberg and W. Kohn, Inhomogeneous electron gas, Phys. Rev. **136**, B864 (1964).

[24] G. Kresse and J. Hafner, *Ab initio* molecular dynamics for liquid metals, Phys. Rev. B **47**, 558 (1993).

[25] G. Kresse and J. Furthmüller, Efficiency of *ab-initio* total energy calculations for metals and semiconductors using a plane-wave basis set, Comput. Mater. Sci. **6**, 15 (1996).

[26] P. E. Blöchl, Projector augmented-wave method, Phys. Rev. B **50**, 17953 (1994).

[27] J. P. Perdew, A. Ruzsinszky, G. I. Csonka, O. A. Vydrov, G. E. Scuseria, L. A. Constantin, X. Zhou, and K. Burke, Restoring the Density-Gradient Expansion for Exchange in Solids and Surfaces, Phys. Rev. Lett. **100**, 136406 (2008).

[28] H. J. Monkhorst and J. D. Pack, Special points for Brillouin-zone integrations, Phys. Rev. B **13**, 5188 (1976).

[29] S. L. Dudarev, G. A. Botton, S. Y. Savrasov, C. J. Humphreys, and A. P. Sutton, Electron-energy-loss spectra and the structural stability of nickel oxide: An LSDA+U study, Phys. Rev. B **57**, 1505 (1998).

[30] B. J. Campbell, H. T. Stokes, D. E. Tanner, and D. M. Hatch, Isodisplace: An internet tool for exploring structural distortions, J. Appl. Cryst. **39**, 607 (2006).

[31] K. Momma and F. Izumi, Vesta 3 for the three-dimensional visualization of crystal, volumetric, and morphology data, J. Appl. Cryst. **44**, 1272 (2011).

[32] A. T. Zayak, X. Huang, J. B. Neaton, and K. M. Rabe, Structural, electronic, and magnetic properties of $SrRuO_3$ under epitaxial strain, Phys. Rev. B **74**, 094104 (2006).

[33] H. D'Hondt, A. M. Abakumov, J. Hadermann, A. S. Kalyuzhnaya, M. G. Rozova, E. V. Antipov, and G. V. Van Tendeloo, Tetrahedral chain order in the $Sr_2Fe_2O_5$ brownmillerite, Chem. Mater. **20**, 7188 (2008).

[34] A. M. Abakumov, A. S. Kalyuzhnaya, M. G. Rozova, E. V. Antipov, J. Hadermann, and G. Van Tendeloo, Compositionally induced phase transition in the $Ca_2MnGa_{1-x}Al_xO_5$ solid solutions: Ordering of tetrahedral chains in the brownmillerite structure, Solid State Sci. **7**, 801 (2005).

[35] J. Hadermann, A. M. Abakumov, H. D'Hondt, A. S. Kalyuzhnaya, M. G. Rozova, M. M. Markina, M. G. Mikheev, N. Tristan, R. Klingeler, B. Büchner, and E. V. Antipov, Synthesis and crystal structure of the $Sr_2Al_{1.07}Mn_{0.93}O_5$ brownmillerite, J. Mater. Chem. **17**, 692 (2007).

[36] T. G. Parsons, H. D'Hondt, J. Hadermann, and M. A. Hayward, Synthesis and structural characterization of $La_{1-x}A_xMnO_{2.5}$(A = Ba,Sr,Ca) phases: Mapping the variants of the brownmillerite structure, Chem. Mater. **21**, 5527 (2009).

[37] A. M. Arevalo-Lopez and J. P. Attfield, Crystal and magnetic structures of the brownmillerite $Ca_2Cr_2O_5$, Dalton Trans. **44**, 10661 (2015).

[38] F. Ramezanipour, J. E. Greedan, A. P. Grosvenor, J. F. Britten, L. M. D. Cranswick, and V. O. Garlea, Intralayer cation ordering in a brownmillerite superstructure: Synthesis, crystal, and magnetic structures of Ca_2FeCoO_5, Chem. Mater. **22**, 6008 (2010).

[39] J. Zhang, H. Zheng, C. D. Malliakas, J. M. Allred, Y. Ren, Q. Li, T.-H. Han, and J. F. Mitchell, Brownmillerite $Ca_2Co_2O_5$: Synthesis, stability, and re-entrant single crystal to single crystal structural transitions, Chem. Mater. **26**, 7172 (2014).

[40] P. A. Maggard, T. S. Nault, S. L. Stern, and K. R. Poeppelmeier, Alignment of acentric $MoO_3F_3^{3-}$ anions in a polar material: $(Ag_3MoO_3F_3)(Ag_3MoO_4)Cl$, J. Solid State Chem. **175**, 27 (2003).

[41] V. M. Goldschmidt, Die gesetze der krystallochemie, Naturwissenschaften **14**, 477 (1926).

[42] Although this is generally intended for use in perovskites, it is also applicable to perovskite-derived structures such as these brownmillerites.

[43] Y. Shimakawa, S. Inoue, M. Haruta, M. Kawai, K. Matsumoto, A. Sakaiguchi, N. Ichikawa, S. Isoda, and H. Kurata, Topotactic changes in thin films of brownmillerite $SrFeO_{2.5}$ grown on $SrTiO_3$ substrates to infinite-layer structure $SrFeO_2$, Cryst. Growth Des. **10**, 4713 (2010).

[44] S. Inoue, M. Kawai, Y. Shimakawa, M. Mizumaki, N. Kawamura, T. Watanabe, Y. Tsujimoto, H. Kageyama, and K. Yoshimura, Single-crystal epitaxial thin films of $SrFeO_2$ with FeO_2 "infinite layers", Appl. Phys. Lett. **92**, 161911 (2008).

[45] M. D. Rossell, O. I. Lebedev, G. V. Van Tendeloo, N. Hayashi, T. Terashima, and M. Takano, Structure of epitaxial $Ca_2Fe_2O_5$ films deposited on different perovskite-type substrates, J. Appl. Phys. **95**, 5145 (2004).

[46] A. M. Glazer, The classification of tilted octahedra in perovskites, Acta. Cryst. **B28**, 3384 (1972).

[47] A. Vailionis, H. Boschker, W. Siemons, E. P. Houwman, D. H. A. Blank, G. Rijnders, and G. Koster, Misfit strain accommodation in epitaxial ABO_3 perovskites: Lattice rotations and lattice modulations, Phys. Rev. B **83**, 064101 (2011).

[48] J. M. Rondinelli and N. A. Spaldin, Structure and properties of functional oxide thin films: Insights from electronic-structure calculations, Adv. Mater. **23**, 3363 (2011).

[49] J. M. Rondinelli, S. J. May, and J. W. Freeland, Control of octahedral connectivity in perovskite oxide heterostructures: An emerging route to multifunctional materials discovery, MRS Bull. **37**, 261 (2012).

[50] R. L. Johnson-Wilke, D. Marincel, S. Zhu, M. P. Warusawithana, A. Hatt, J. Sayre, K. T. Delaney, R. Engel-Herbert, C. M. Schlepütz, J.-W. Kim, V. Gopalan, N. A. Spaldin, D. G. Schlom, P. J. Ryan, and S. Trolier-McKinstry, Quantification of octahedral rotations in strained $LaAlO_3$ films via synchrotron x-ray diffraction, Phys. Rev. B **88**, 174101 (2013).

[51] H. W. Eng, P. W. Barnes, B. M. Auer, and P. M. Woodward, Investigations of the electronic structure of d^0 transition metal oxides belonging to the perovskite family, J. Solid State Chem. **175**, 94 (2003).

[52] A. Amat, E. Mosconi, E. Ronca, C. Quarti, P. Umari, M. K. Nazeeruddin, M. Grätael, and F. D. Angelis, Cation-induced band-gap tuning in organohalide perovskites: Interplay of spin-orbit coupling and octahedra tilting, Nano Lett. **14**, 3608 (2014).

[53] M. Filip, G. E. Eperon, H. J. Snaith, and F. Giustino, Steric engineering of metal-halide perovskites with tunable optical band gaps, Nature Commun. **5**, 5757 (2014).

[54] U. Aschauer and N. A. Spaldin, Competition and cooperation between antiferrodistortive and ferroelectric instabilities in the model perovskite $SrTiO_3$, J. Phys.: Condens. Matter **26**, 122203 (2014).

[55] H. Li, I. E. Castelli, K. S. Thygesen, and K. W. Jacobsen, Strain sensitivity of band gaps of sn-containing semiconductors, Phys. Rev. B **91**, 045204 (2015).

[56] M. Imada, A. Fujimori, and Y. Tokura, Metal-insulator transitions, Rev. Mod. Phys. **70**, 1039 (1998).